CHEMISTRY OF MATERIALS
Cite This: Chem. Mater. 2017, 29, 8757-8765
Article
pubs.acs.org/cm

Bioresponsive Chimaeric Nanopolymersomes Enable Targeted and Efficacious Protein Therapy for Human Lung Cancers *in Vivo*

Weijing Yang, Yifeng Xia, Yan Zou, Fenghua Meng,* Jian Zhang, and Zhiyuan Zhong*

Biomedical Polymers Laboratory, College of Chemistry, Chemical Engineering and Materials Science, and Key Laboratory of Stem Cells and Biomedical Materials of Jiangsu Province and Chinese Ministry of Science and Technology, Soochow University, Suzhou, 215123, P. R. China

Supporting Information

ABSTRACT: Rapidly evolving protein technology has generated hundreds of therapeutic proteins that are promising for treating various human diseases. The clinical use of protein drugs remains, however, limited due to the absence of viable vehicles. Here, we report that anisamide-functionalized bioresponsive chimaeric nanopolymersomes (Anis-BCPs) can efficiently load granzyme B (GrB), a potent apoptotic protein, and enable targeted and efficacious protein therapy for H460 human lung cancer *in vivo*. Anis-BCPs are readily obtained from poly(ethylene glycol)-*b*-poly(*N*-2-hydroxypropyl methacrylamide-*g*-lipoic acid)-*b*-poly(acrylic acid) triblock copolymer. Notably, GrB-loaded Anis-BCPs a display superior antitumor effect toward sigma receptor-overexpressing H460 lung cancer cells (IC_{50} = 7.8 nM). The *in vivo* studies reveal that Anis-BCPs have a long circulation time and remarkable tumor accumulation. Interestingly, GrB-loaded Anis-BCPs at 6.24 nmol GrB equiv/kg dose, given either in four injections or one single injection, effectively inhibit H460 tumor growth and significantly improve the survival rate for mice. These robust, bioresponsive, and nontoxic chimaeric nanopolymersomes provide a potential platform for cancer protein therapy as well as basic research on intracellular functional proteins.

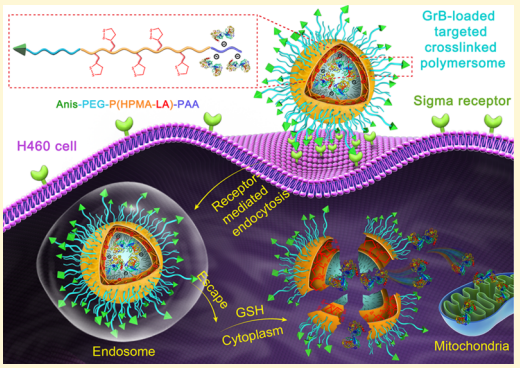

1. INTRODUCTION

Protein therapy has promised to offer revolutionary treatment for various human diseases.[1−5] Rapidly evolving protein technology has generated hundreds of potent therapeutic proteins. It is recognized that protein drugs usually possess a better specificity and are generally safer than chemotherapeutics. The direct injection of protein therapeutics, however, results in a typically poor treatment effect owing to their particular fragility *in vivo*.[6] For many protein drugs like cytochrome C (CC) and granzyme B (GrB) that are taking effect inside the cancer cells, cell penetration and intracellular trafficking present additional challenges.[7,8] The clinical translation of protein drugs relies on advancement of clinically viable nanocarriers. Different responsive nanocarrier systems like capsules, nanogels, and micellar nanocomplexes have recently been exploited for anticancer drug delivery[9−11] and especially for protein delivery.[12−23] However, in spite of significant progress made on intracellular protein chaperones, there are few reports on cancer protein therapy *in vivo*.[12,13,24]

Nanopolymersomes containing an aqueous lumen[25−30] that can load and protect water-soluble biopharmaceutics are among the most ideal protein nanocarriers.[31−33] Discher et al. reported that insulin encapsulated in polymersomes had a prolonged circulation and was released in a controlled manner.[34] van Hest et al. reported that TAT modified polymersomes could load GFP (green fluorescent protein) and HRP (horseradish peroxidase) and improve their stability and cellular uptake.[35] Nevertheless, polymersomes typically had a low protein-loading efficiency and content. Interestingly, chimaeric polymersomes could significantly improve protein loading and intracellular protein delivery *in vitro*.[36,37]

Here, we report that anisamide-functionalized bioresponsive chimaeric nanopolymersomes (Anis-BCPs) efficiently load GrB and enable targeted and efficacious protein therapy for H460 human lung cancers *in vivo*. Anis-BCPs are readily obtained from triblock copolymers poly(ethylene glycol)-*b*-poly(*N*-2-hydroxypropyl methacrylamide-*g*-lipoic acid)-*b*-poly(acrylic acid) (PEG-P(HPMA-LA)-PAA) and Anis-PEG-P(HPMA-LA)-PAA (Figure 1). Notably, PEG, PHPMA, and PAA are well-known biocompatible and water-soluble polymers[38] while LA is an endogenous antioxidant existing in the human body.[39,40] The conjugation of PHPMA with LA makes the water-soluble triblock copolymers become vesicle-forming amphiphiles. Interestingly, by employing the unique ring-opening polymerization feature of LA, we have obtained reversibly cross-linked nanoparticles, micelles, and polymersomes for enhanced delivery of hydrophobic and hydrophilic chemotherapeutics.[41,42] Anis with a high affinity to sigma

Received: July 14, 2017
Revised: September 29, 2017
Published: September 29, 2017

DOI: 10.1021/acs.chemmater.7b02953
Chem. Mater. 2017, 29, 8757−8765

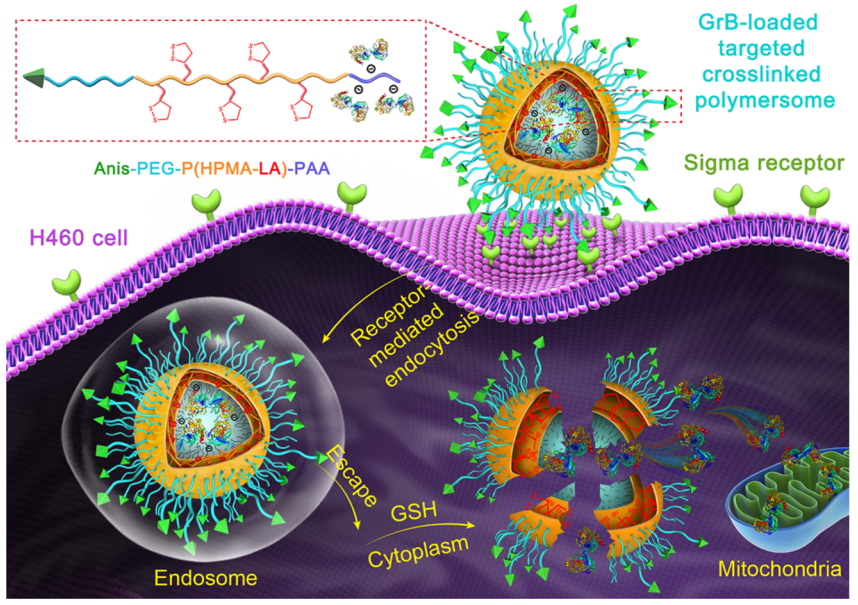

Figure 1. Schematic presentation of GrB-Anis-BCPs for efficient loading, receptor-mediated internalization, and intracellular GSH-triggered release of GrB in sigma receptor-overexpressing H460 lung cancer cells.

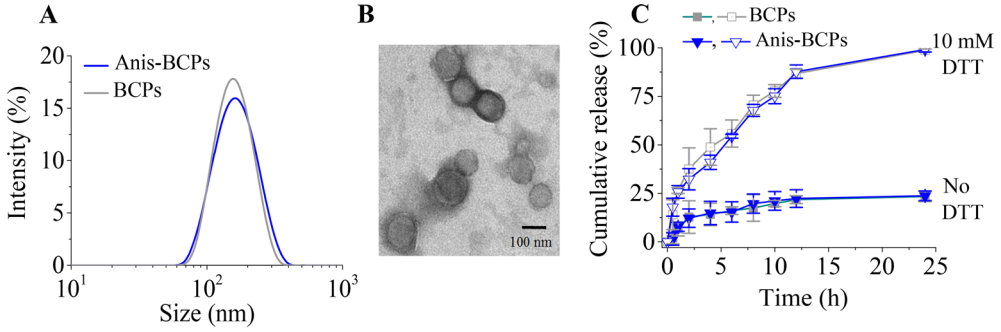

Figure 2. Size and size distribution of Anis-BCPs measured by (A) DLS and (B) TEM. (C) The *in vitro* FITC-CC release from Anis-BCPs in the presence or absence of 10 mM DTT in PBS (pH 7.4) at 37 °C and polymersome concentration of 80 μg/mL (n = 3).

receptors has shown effective targeting ability to several human malignancies including lung and prostate cancers.[13,43,44] This represents a first development of smart polymersomes that are capable of efficient protein loading and cancer-targeting protein therapy *in vivo*.

2. RESULTS AND DISCUSSION

2.1. Fabrication and Protein Loading of Bioresponsive Chimaeric Polymersomes. Anis-BCPs were readily co-self-assembled from PEG-P(HPMA-LA)-PAA and Anis-PEG-P(HPMA-LA)-PAA that were synthesized by sequential RAFT polymerization of HPMA and AA in the presence of MeO-PEG-CPADN (M_n = 5.0 kg/mol) or Anis-PEG-CPADN (M_n = 7.5 kg/mol) followed by lipoylation (Scheme S1). ^{1}H NMR analyses revealed that PEG-PHPMA-PAA had an M_n of 5.0−9.0−2.4 kg/mol (Figure S1A, Table S1). GPC curve showed a narrow molecular weight distribution ($Đ$) of 1.07. Similarly, Anis-PEG-PHPMA-PAA was obtained with an M_n of 7.5−9.2−2.4 kg/mol and $Đ$ of 1.14. The lipoylation of PEG-PHPMA-PAA and Anis-PEG-PHPMA-PAA yielded PEG-P(HPMA-LA)-PAA and Anis-PEG-P(HPMA-LA)-PAA with degrees of substitution (DS) of LA of 75 and 67, respectively, as determined by ^{1}H NMR (Figure S1B, Figure S2).

Anis-BCPs with different targeting densities were prepared at varying Anis-PEG -P(HPMA-LA)-PAA molar percentages from 18.5% to 67.9% followed by adding catalytic 1,4-dithio-D,L-threitol (DTT). The sizes of polymersomes increased slightly with Anis densities, from 156 to 167 nm with polydispersity indexes (PDIs) of 0.12−0.19 (Table S2 and Figure 2A). Anis-BCPs with 47.6% Anis can serve as an example. The TEM micrograph revealed a spherical morphology and vesicular structure (Figure 2B). UV spectra demonstrated the disappearance of dithiolane absorbance at 310 nm confirming the occurrence of disulfide cross-linking in Anis-BCPs (Figure S3A). Anis-BCPs displayed a slightly negative surface charge of −8.7 mV (Table S2), supporting that a short PAA block is preferentially located in the lumen. We and others have demonstrated that asymmetric triblock copolymers tend to form chimaeric vesicles.[45,46] Anis-BCPs are stable under low concentration and high salt condition (Figure S3B). However, upon addition of 10 mM glutathione (GSH), Anis-BCPs formed large aggregates and precipitates in 24 h (Figure S3C), verifying that Anis-BCPs have a fast response to reduction conditions. The nontargeting BCPs had similar size, zeta potential, and reduction responsivity.

FITC-labeled cytochrome C (FITC-CC), as a model protein, could be efficiently encapsulated into Anis-BCPs with protein-

DOI: 10.1021/acs.chemmater.7b02953
Chem. Mater. 2017, 29, 8757−8765

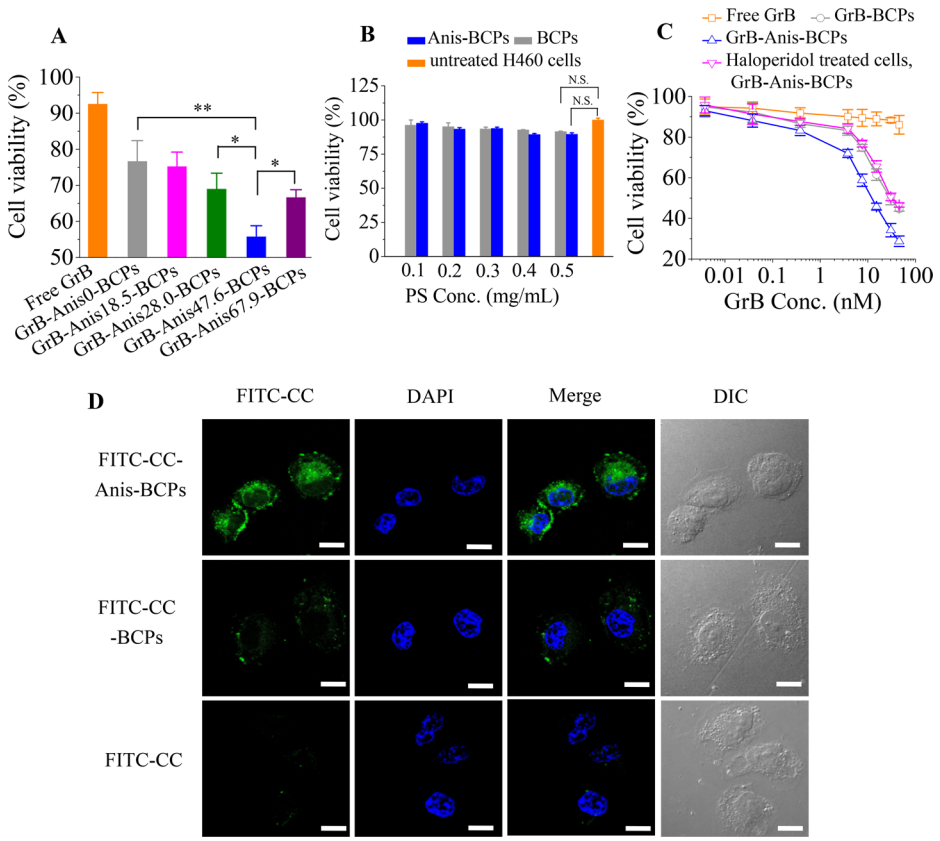

Figure 3. (A) Cytotoxicity of GrB-Anis-BCPs at Anis content from 0%, 18.5%, 28.0%, 47.6%, to 67.9% to H460 cells determined by MTT assays (GrB dosage: 12.5 nM). Free GrB was used as a control. (B) The cell viability of empty BCPs and Anis-BCPs (Anis density: 47.6%) at 48 h incubation (n = 4). (C) MTT assays of GrB-Anis-BCPs, GrB-BCPs, and free GrB (GrB dosage: 0.003−37.5 nM) on H460 cells (n = 4). H460 cells pretreated with 30 μM haloperidol for 3 h were used as controls. (D) CLSM images of H460 cells at 12 h incubation with FITC-CC formulations (FITC-CC dosage: 3.85 μM). Scale bar: 15 μm. For parts A and C, the cells were incubated 4 h with samples, the medium was replaced with fresh culture medium, and the cells were further cultivated for 68 h. n = 4. One-way ANOVA with Tukey multiple comparison tests, $p > 0.05$ means not significant (N.S.), $*p < 0.05$, $**p < 0.01$.

loading efficiencies (PLE) exceeding 96% at theoretical protein-loading contents (PLC) of 1.0−5.0 wt % (Table S3). This is probably due to the electrostatic interaction between positively charged FITC-CC and PAA in the lumen as well as the protection from highly stable polymersome membrane. Anis-BCPs achieved a striking PLC of 36.5 wt % at a theoretical PLC of 50 wt %. FITC-CC-loading had not much influence on the size, size distribution, and surface charge of Anis-BCPs. GrB-loaded Anis-BCPs (GrB-Anis-BCPs) at a theoretical PLC of 2.4 wt % exhibited also similar size and zeta potential to those of FITC-CC-Anis-BCPs (Table S4). Notably, Figure 2C shows that less than 20% protein was released from FITC-CC-loaded Anis-BCPs in 24 h under physiological conditions, while protein release was quantitative under a reductive condition containing 10 mM DTT. Hence, Anis-BCPs can not only efficiently load protein but also achieve fast responsive protein release.

2.2. Cell Selectivity and Antitumor Activity of GrB-Anis-BCPs. We first used flow cytometric analyses to determine the expression of sigma receptor on H460 cells using sigma receptor antibody as a primary antibody. The results clearly showed that H460 cells had over 3-fold higher sigma receptor expression than A549 and MCF-7 cells (Figure S4), verifying that H460 lung cancer cells overexpress sigma receptors.[47] Thus, H460 cells were used to evaluate the polymersome behavior *in vitro* and *in vivo*. To investigate the effect of Anis surface density on the anticancer activity of Anis-BCPs, we conducted MTT studies of GrB-Anis-BCPs with varying Anis densities from 0%, 18.5%, 28.0%, 47.6%, to 67.9%. The results displayed that GrB-Anis-BCPs with 47.6% Anis had the highest anticancer activity (Figure 3A). In the following, we selected Anis-BCPs with 47.6% Anis for further *in vitro* and *in vivo* studies if not indicated otherwise. Besides, the MTT assay results (Figure 3B) confirmed that empty Anis-BCPs and BCPs did not cause significant cytotoxicity to H460 cells even at 0.5 mg/mL as compared to PBS (P = 0.07).

Further MTT assays showed that free GrB induced little H460 cell death due to poor cell penetration as also reported previously.[48] However, GrB-Anis-BCPs exhibited a remarkably high antitumor effect toward H460 cells with an IC_{50} as low as 7.8 nM (Figure 3C). This IC_{50} was over 4-fold lower than fusion protein GrB/scFvMEL to the most sensitive A375-M cells[49] and 12.8-fold lower than p53 protein-loaded nanocapsules toward MDA-MB-231 cells,[50] respectively. The nontargeted control, GrB-BCPs, though less potent than GrB-Anis-BCPs, could also inhibit cell growth (IC_{50} = 27.2 nM). The pretreatment of H460 cells with free haloperidol (antagonist to σ receptors)[45,48] reduced the cytotoxicity of GrB-Anis-BCPs to the level of GrB-BCPs (Figure 3C). These results confirm that GrB-Anis-BCPs can actively target H460 cells.

DOI: 10.1021/acs.chemmater.7b02953
Chem. Mater. 2017, 29, 8757−8765

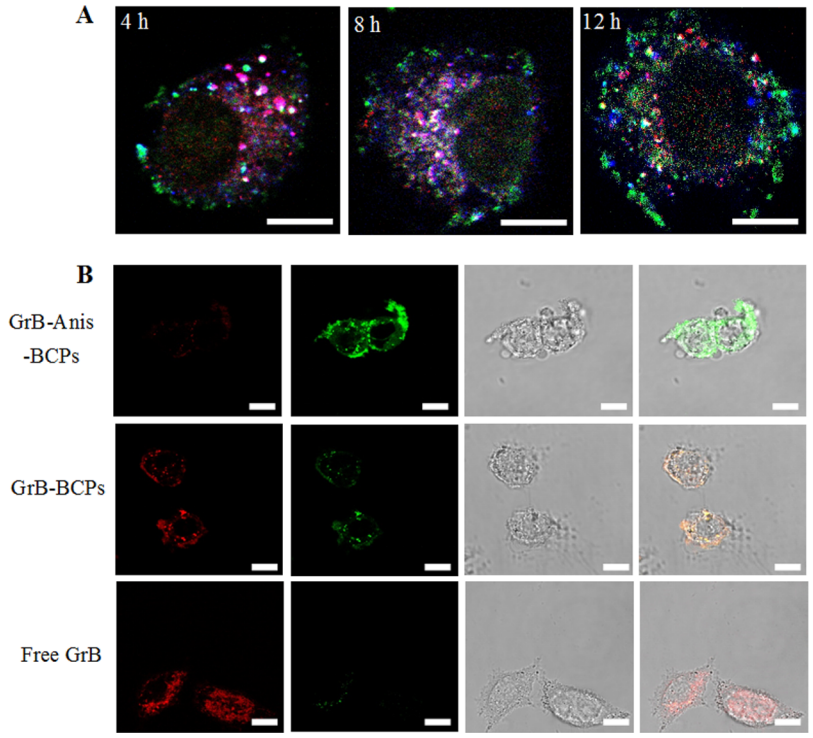

Figure 4. CLSM observation of intracellular protein trafficking pathway with Anis-BCPs. (A) H460 cells following 4, 8, or 12 h incubation with FITC-CC-Anis-BCPs-Cy5. Green, blue, and red are FITC-CC, Cy5-labeled polymersomes, and endo/lysosomes, respectively ([FITC-CC] = 3.85 μM). (B) MitoCapture stained H460 cells after incubation with different GrB formulations ([GrB] = 12.5 nM) for 24 h. For each panel, images from left to right: MitoCapture stained mitochondrial membrane (red), MitoCapture released in cytosol (green), DIC images, and overlays of the above images. Scale bars: 15 μm.

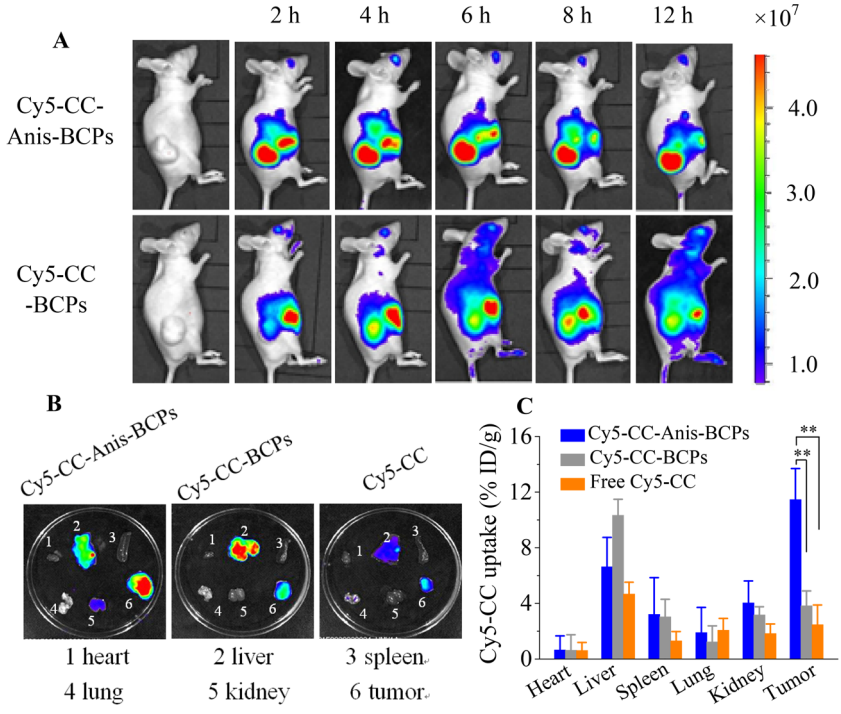

Figure 5. *In vivo* biodistribution of Cy5-CC-Anis-BCPs in nude mice bearing H460 xenografts (Cy5 dosage: 0.4 μmol Cy5/kg). (A) The *in vivo* images of the mice treated with Cy5-CC-Anis-BCPs and Cy5-CC-BCPs. The *ex vivo* fluorescence images (B) and quantitative biodistribution (C) of tumors and major organs of the mice treated with Cy5-CC-Anis-BCPs, Cy5-CC-BCPs, and free Cy5-CC at 8 h post-iv-injection. n = 3, one-way ANOVA with Tukey multiple comparison tests, $^{**}p < 0.01$.

The cellular internalization and protein release of Anis-BCPs was studied by a confocal scanning microscope (CLSM) using FITC-CC as a model protein. Figure 3D shows that H460 cells after 12 h of treatment with FITC-CC-Anis-BCPs gave strong

DOI: 10.1021/acs.chemmater.7b02953
Chem. Mater. 2017, 29, 8757−8765

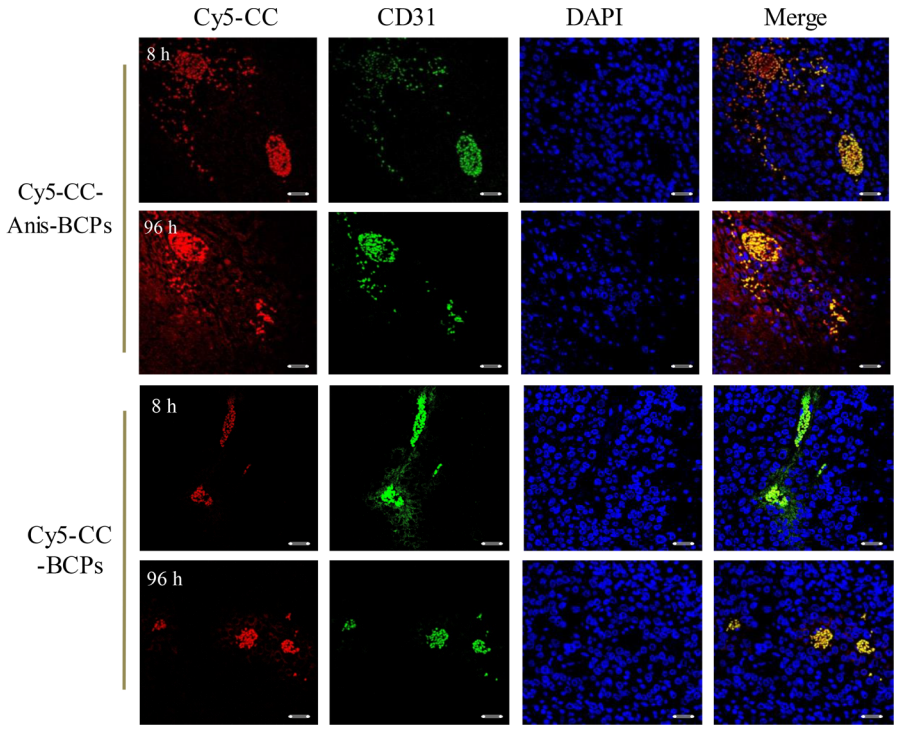

Figure 6. Distribution of Cy5-CC in tumor tissue near the tumor center area of mice following 8 or 96 h treatment with Cy5-CC-Anis-BCPs and Cy5-CC-BCPs (0.4 μmol Cy5 equiv/kg). The blood vessels were treated with rat antimouse CD31 antibody and then by Alexa fluor 488 goat antirat secondary antibody. The cell nuclei were stained with DAPI. Scale bar: 100 μm.

FITC fluorescence, whereas weak and no FITC fluorescence was discerned in H460 cells treated with nontargeted FITC-CC-BCPs and free FITC-CC, respectively, supporting that Anis-BCPs can efficiently transport and release protein into H460 cells. Further studies by labeling the endo/lysosomes with lysotracker-red (red), proteins with FITC (green), and polymersomes with Cy5 (blue) showed that with prolonging the incubation time the colocalization of proteins and polymersomes and lysosomes (white), proteins and polymersomes (light blue), and polymersomes and lysosomes (pink) decreased greatly, and a large amount of separated protein green dots was clearly observed, indicating effective endosomal escape and fast protein release from FITC-CC-Anis-BCPs inside H460 cells (Figure 4A).

The effect of released GrB on mitochondrial membrane of H460 cells was studied using a MitoCapture Kit. CLSM observations showed that free GrB treated H460 cells after MitoCapture staining had only red fluorescence (Figure 4B), implying that mitochondrial membranes were intact.[51] In comparison, cells treated by GrB-BCPs revealed both red and green fluorescence, indicating some damage to mitochondrial membranes. Notably, GrB-Anis-BCP treated cells displayed strong green fluorescence, supporting a high permeability of mitochondrial membranes. Therefore, cytosolic released GrB from Anis-BCPs could effectively target mitochondria and cause the pore-formation in the mitochondrial membranes, which would in turn lead to release of apoptotic effectors like SMACs or CC into the cytosol.[52]

2.3. *In Vivo* Pharmacokinetics and Biodistribution of Protein-Loaded Polymersomes. In order to study the pharmacokinetics, we labeled bare polymersomes with Cy5. Figure S5 shows that both Anis-BCPs-Cy5 and BCPs-Cy5 had a long circulation time with elimination phase half-lives ($t_{1/2,\beta}$) of 6.32 and 6.10 h, respectively. For biodistribution studies, Anis-BCPs were loaded with Cy5-labeled CC (Cy5-CC-Anis-BCPs). Interestingly, the *in vivo* imaging showed that Cy5-CC-Anis-BCPs treated mice started to show strong fluorescence at 2 h postinjection, and the fluorescence remained high until 12 h (Figure 5A). In comparison, significantly lower tumor accumulation was observed for Cy5-CC-BCPs. The *ex vivo* fluorescence images of the major organs and tumors isolated at 8 h postinjection revealed that mice treated with Cy5-CC-Anis-BCPs had significantly stronger tumor Cy5-CC fluorescence than those with Cy5-CC-BCPs and free Cy5-CC controls (Figure 5B). Notably, the tumors of mice treated with Cy5-CC-Anis-BCPs had the strongest Cy5-CC fluorescence among all major organs. Quantitative analyses of Cy5-CC fluorescence showed a high Cy5-CC accumulation of 11.5% ID/g in tumors at 8 h postinjection of Cy5-CC-Anis-BCPs, which was about 2.5- and 5.2-fold higher than those treated with Cy5-CC-BCPs (4.1% ID/g) and free Cy5-CC (2.1% ID/g), respectively (Figure 5C). The tumor-to-normal tissue (T/N) ratios of Cy5-CC-Anis-BCPs treated mice were ca. 2.0−5.0 times higher than those with Cy5-CC-BCPs and Cy5-CC (Table S5).

We further studied the tumor penetration property of Cy5-CC-Anis-BCPs after a single iv injection. Figure 6 shows the CLSM images tumor tissues near the tumor central area. It was found that at 8 h postinjection strong Cy5-CC fluorescence (red) was observed, and it colocalized with the blood vessels (green). Notably, at 96 h postinjection, a significant amount of Cy5-CC fluorescence distributed throughout the whole tumor slices and inside the tumor cells (Figure 6). In contrast, although Cy5-CC strongly accumulated in the blood vessels at 96 h, very low Cy5-CC fluorescence was detected out of the blood vessels, and very little was inside the tumor cells in the tumor slices from Cy5-CC-BCPs treated mice (Figure 6). Hence, Anis functionalization has not only improved the tumor

DOI: 10.1021/acs.chemmater.7b02953
Chem. Mater. 2017, 29, 8757−8765

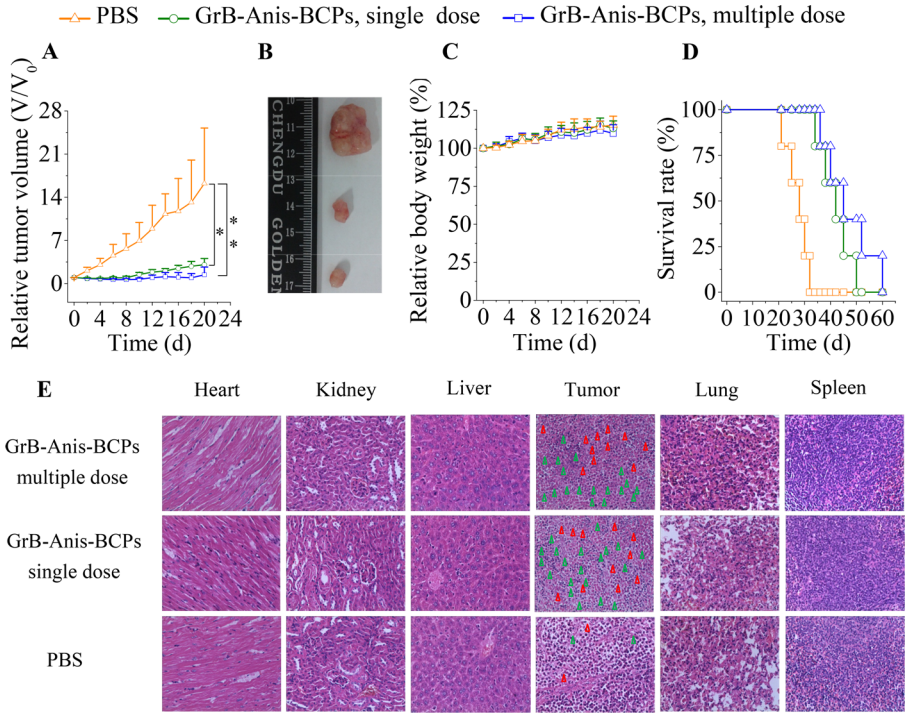

Figure 7. *In vivo* therapeutic effect of H460 tumor-bearing nude mice using GrB-Anis-BCPs. The mice were treated with multiple dose of GrB-Anis-BCPs at 1.56 nmol GrB/kg on day 0, 4, 8, and 12, or with a single dose at 6.24 nmol GrB/kg on day 0. PBS was used as a control. (A) Tumor volume changes in 20 days (n = 6, one-way ANOVA with Tukey multiple comparison tests, *p < 0.05, **p < 0.01). (B) Photograph of tumors on day 20. (C) Body weight changes in 20 days (n = 6). (D) Survival rates of mice (n = 5). (E) H&E stained sections of major organs and tumors on day 20 (400×). The green and red triangles point to apoptotic and necrotic cells, respectively.

accumulation of Cy5-CC-BCPs but also led to enhanced tumor penetration and superior tumor cell uptake.

2.4. Therapeutic Efficacy of GrB-Anis-BCPs in H460 Tumor-Bearing Mice. We evaluated the *in vivo* therapeutic efficacy of GrB-Anis-BCPs in H460 tumor xenografts. In a preliminary experiment, mice were treated with GrB-Anis-BCPs at a dosage of 1.56 nmol GrB equiv/kg, given every 4 days for a total of four injections. The results showed complete tumor growth inhibition (Figure S6A,B). In contrast, the nontargeting GrB-BCPs were much less potent, likely due to their inferior tumor penetration and tumor cell uptake. The empty Anis-BCPs, as expected, had no any inhibitive effect. Interestingly, a single dose of GrB-Anis-BCPs at 1.56 nmol GrB/kg revealed slightly better tumor inhibition than multiple doses of GrB-BCPs. Figure S6C shows no body weight loss for all treatments, suggesting low systemic toxicity of Anis-BCPs, either with or without loading of GrB.

In the next, we investigated the treatment effect of GrB-Anis-BCPs in H460 tumor-bearing nude mice at a single dose of 6.24 nmol GrB/kg or multiple doses (4 × 1.56 nmol GrB/kg) (n = 6). Interestingly, both treatment schemes effectively suppressed tumor growth (Figure 7A). The photograph of tumors isolated on day 20 confirmed similar tumor inhibition by either single or multiple doses (Figure 7B). Notably, both treatment schemes led to no loss of body weight (Figure 7C). Figure 7D reveals that treatment with GrB-Anis-BCPs markedly prolonged the survival rate of the mice, with a median survival time of 42−45 days versus 28 days for the PBS group. GrB is a potent apoptosis inducer, but the particularly poor cell entry restricts it from direct applications. Fusion proteins like GrB/antibody[53] and GrB/VEGF$_{121}$[54] were designed to increase the specific cellular uptake and inhibit tumor growth *in vivo*, though at a 7.5−134-fold higher GrB dose than GrB-Anis-BCPs. GrB-loaded hyaluronic acid nanogels were able to inhibit breast and lung tumor growth at 2.4−3.7-fold higher GrB dose than GrB-Anis-BCPs.[24] The high antitumor effect of GrB-Anis-BCPs is likely due to their improved protection of proteins from degradation in circulation, high tumor accumulation, efficient cell uptake, and fast intracellular protein release. H&E staining showed that GrB-Anis-BCPs induced extensive apoptosis (green triangles) and necrosis (red triangles) in the tumors with prominent cell membrane shrinkage and nuclear fragmentation with no damage to the major organs (heart, kidney liver, lung, and spleen) (Figure 7E), supporting that GrB-Anis-BCPs have an excellent safety profile.

3. CONCLUSION

We have demonstrated that anisamide-functionalized bioresponsive chimaeric nanopolymersomes (Anis-BCPs) can efficiently load and deliver apoptotic proteins into the cytosol of sigma receptor-overexpressing H460 cells *in vitro* and *in vivo*, inducing potent lung tumor suppression with little side effects. This is the first report on development of smart polymersomes for efficacious and targeted cancer protein therapy *in vivo*. Anis-BCPs have several advantages for cancer protein therapy. First, their chimaeric structure allows efficient loading of proteins into the lumen as well as protection of loaded proteins from degradation. Second, they can selectively target and be internalized by sigma receptor-overexpressing cancer cells. Third, proteins can be quickly released under cytoplasmic-mimicking reductive environment, inducing a high apoptotic effect. Notably, GrB-Anis-BCPs displayed a remarkably low IC$_{50}$ of 7.8 nM to H460 cells. GrB-Anis-BCPs caused complete H460 tumor growth inhibition at a low dosage of 6.24 nmol

DOI: 10.1021/acs.chemmater.7b02953
Chem. Mater. 2017, 29, 8757−8765

GrB equiv/kg, which was 7.5−134-fold lower than GrB fusion protein constructs.[53,54] Finally, as compared to most protein nanocarriers, GrB-Anis-BCPs are particularly simple and easy to fabricate under mild conditions, which render them interesting for clinical translation. The facile loading and efficient intracellular chaperone of proteins also makes BCPs an appealing tool to unveil the intracellular behaviors and functions of various biologically active proteins. Anis-BCPs have appeared as a novel and efficient platform for targeted cancer protein therapy as well as basic research on intracellular functional proteins.

4. EXPERIMENTAL SECTION

4.1. Preparation of Anis-BCPs and Protein-Loaded Anis-BCPs. A 50 μL portion of DMSO solution (5 mg/mL) of Anis-PEG-P(HPMA-LA)-PAA and PEG-P(HPMA-LA)-PAA at a predetermined molar ratio was injected into 0.95 mL of phosphate buffer (PB, pH 7.4, 5 mM). After keeping still for 2 h, a homogeneous bluish dispersion was obtained. Under a nitrogen atmosphere, 10 mol % DTT relative to the lipoyl units was added (final concentration: 0.05 mM) to cross-link the polymersomes.[42] The mixture was stirred for 12 h at room temperature (rt) and dialyzed against PB for 12 h (MWCO 3500), yielding Anis-functionalized bioresponsive chimaeric nanopolymersomes (Anis-BCPs). The colloidal stability of Anis-BCPs against large dilution, in solution containing high salt concentration or in cell culture medium, was tracked by dynamic light scattering (DLS).

Protein-loaded Anis-BCPs were prepared similarly except that PB was replaced by recombinant human granzyme B (GrB), FITC-labeled cytochrome C (FITC-CC), or Cy5-labeled cytochrome C (Cy5-CC) solution in PB, and extensive dialysis using a regenerated cellulose membrane of MWCO 300 000 Da was conducted. FITC-CC was used at varying theoretical loading contents from 1 to 50 wt % relative to the copolymers used. The protein loading and release were described in detail in Supporting Information.

4.2. MTT Assays. The sigma receptor-overexpressing H460 cells were cultured in 96-well plates (3×10^3 cells/well) using RPMI-1640 medium supplemented with 10% fetal bovine serum (FBS), 1% L-glutamine, and antibiotics penicillin (100 IU/mL) and streptomycin (100 μg/mL) for 24 h in an atmosphere containing 5% CO_2 at 37 °C. GrB-Anis-BCPs, GrB-BCPs, or free GrB (protein concentrations ranging from 0.003 to 37.5 nM) in 20 μL of PBS was added and incubated for 4 h. PBS was used as control. Then, the cell culture medium was replaced with fresh medium, and the cells were cultured for another 68 h. A PBS solution of 3-(4,5-dimethylthiazol-2-yl)-2,5-diphenyl- tetrazolium bromide (MTT) (10 μL, 5.0 mg/mL) was added to each well. After incubation for 4 h, the MTT-formazan generated by live cells was dissolved in 150 μL of DMSO for 20 min. The absorbance at 570 nm was measured using a microplate reader (Multiskan FC). The cell viability (%) was determined by comparing the absorbance at 570 nm of each wells with those of control wells treated with PBS. Data are presented as average ± SD ($n = 4$).

To perform competitive inhibition experiments, H460 cells were treated with 30 μM haloperidol for 3 h,[43] and the medium was replaced by fresh culture medium before GrB-Anis-BCPs were added.

The cytotoxicity of empty Anis-BCPs and BCPs to H460 cells was determined similarly by incubating polymersomes (final concentrations of 0.1, 0.2, 0.3, 0.4, and 0.5 mg/mL) for 48 h at 37 °C.

4.3. Confocal Laser Scanning Microscope (CLSM) Studies. H460 cells were cultured on microscope coverslips in 24-well plates (5×10^4 cells/well). To study cellular uptake and intracellular protein release, the cells were incubated with FITC-CC-Anis-BCPs, FITC-CC-BCPs, or free FITC-CC (GrB dosage: 3.85 μM) in 100 μL of PBS at 37 °C for 12 h. The culture medium was removed, and the cells on microscope coverslips were washed with PBS (3×) before fixation with 4% formaldehyde for 15 min and PBS washing (3×). The cell nuclei were stained with 4′,6-diamidino-2-phenyl-indole (DAPI) for 10 min followed by PBS washing (3×). CLSM images of cells were obtained using TCS SP5.

To investigate the endosomal escape, H460 cells in 24-well plates were incubated with FITC-CC-Anis-BCPs-Cy5 (FITC-CC dosage, 3.85 μM; FITC, 7.20 nmol equiv/mL; Cy5, 4.06 nmol Cy5 equiv/mL) for 4, 8, or 12 h. The media were removed, and the cells on microscope coverslips were washed with PBS (3×). Then endosomes were stained with lysotracker-red (100 μL, 150 nM) for 50 min, followed by PBS washing (3×), fixation with 4% formaldehyde for 15 min, and PBS washing (3×). The cell nuclei were stained with DAPI for 10 min followed by PBS washing (3×) before taking CLSM.

For determination of the miochondrial membrane potential ($\Delta\Psi_m$), H460 cells cultured in 8-well glass slide plate (3×10^4 cells/well) were incubated with 60 μL of GrB-Anis-BCPs, GrB-BCPs, or free GrB (GrB dosage: 12.5 nM) for 4 h. The medium was removed and replaced with fresh medium, and the cells were further cultured for 20 h. The cells were stained with 1 mL of MitoCapture dye solution for 15 min according to the manual and washed with PBS before CLSM observation.

4.4. Animal Models. All animal experiments were approved by the Animal Care and Use Committee of Soochow University (P. R. China), and all protocols of animal studies conformed to the Guide for the Care and Use of Laboratory Animals. Mice bearing H460 tumor xenografts were built by subcutaneous injection of 0.05 mL of H460 cell suspension (1×10^7 cells) into the right hind flank of the female nude mice (18−22 g). Tumor inhibition experiments started when the tumors reached 100 mm^3 after ca. 2 weeks. At tumor size of 150−200 mm^3, the penetration of the polymersomes into tumor tissues was studied. The *in vivo* imaging and biodistribution experiments were conducted at tumor size of 200−300 mm^3.

4.5. *In Vivo* Fluorescence Imaging and Biodistribution of Cy5-CC-Anis-BCPs in Mice. To study the *in vivo* imaging and biodistribution, Cy5-CC-loaded polymersomes, Cy5-CC-Anis-BCPs, and Cy5-CC-BCPs were used for detection. To monitor the *in vivo* imaging of proteins, 0.2 mL of PBS solution of Cy5-CC-Anis-BCPs and Cy5-CC-BCPs were iv injected via tail veins into the H460 tumor-bearing mice (0.4 μmol Cy5 equiv/kg). At 2, 4, 6, 8, and 12 h postinjection, the mice were scanned using an IVIS II fluorescence imaging system. For *ex vivo* imaging, the mice were sacrificed, and the tumors and major organs were excised, washed, dried with paper towel, and subjected to fluorescence images with IVIS II.

To quantify Cy5-CC biodistribution, the tumors and organs were homogenized in 0.4 mL of 1% triton X-100 with a homogenizer (IKA T25). Each tissue lysate was incubated with 0.6 mL of extraction solution (DMSO containing 20 mM DTT) in a shaking bath (37 °C, 200 rpm). After centrifugation (14.8 krpm, 30 min), Cy5-CC concentration in the supernatant was determined by fluorometry based on a calibration curve, and expressed as percentage injected dose per gram of tissue (% ID/g).

4.6. Tumor Penetration of Anis-BCPs. Cy5-CC-Anis-BCPs were used to track the location of proteins in the tumors. A single dose of Cy5-CC-Anis-BCPs or Cy5-CC-BCPs in 0.2 mL of PBS (0.4 μmol Cy5 equiv/kg) was injected via tail veins into H460 tumor-bearing mice. At 8 and 96 h postinjection, the mice were sacrificed, and the tumor blocks were excised, washed, dried with paper towel, fixed with 10% formalin, and embedded in paraffin. The tumors were then sliced (thickness: 4 μm), and the sliced tissues were mounted on glass slides. The blood vessels in the tumor tissues were first treated with rat antimouse CD31 antibody and then by Alexa fluor 488 goat antirat secondary antibody according to the manual. The cell nuclei were stained with DAPI. The proteins (red), blood vessels (green), and cell nuclei (blue) in the center region and periphery of tumor slices were observed under a CLSM (20× objective).

4.7. *In Vivo* Treatment of H460 Lung Cancer with GrB-Anis-BCPs. The H460 tumor-bearing mice were weighed and randomly divided into three groups ($n = 6$). The effect of multidose or a single dose of GrB-Anis-BCPs (total dose: 6.24 nmol GrB/kg) on the antitumor efficacy was investigated. GrB-Anis-BCPs (single dose: 6.24 nmol GrB/kg), GrB-Anis-BCPs (multiple dose: 4 × 1.56 nmol GrB/kg), and PBS were iv injected via the tail veins either on day 0 only, or on day 0, 4, 8, and 12. The tumor size was measured using calipers every 2 days, and tumor volume (V) was calculated according to the

DOI: 10.1021/acs.chemmater.7b02953
Chem. Mater. 2017, 29, 8757−8765

formula $V = 0.5 \times L \times W^2$, wherein L and W are the tumor dimension at the longest and widest point, respectively. The relative tumor volume was calculated as V/V_0 (V_0: tumor volume on day 0). The body weight of mice was measured every 2 days, and the relative body weight was normalized to the initial weights.

On day 20, one mouse of each group was sacrificed, and the tumors and major organs were taken and prepared for photographs and histological analyses. The rest of the mice (n = 5) were used to determine the survival rates within 60 days. Mice in each cohort were considered to be dead either when the mice died during treatment or when the tumor volume reached 2000 mm^3.

For histological analyses, the excised tumors and organs were fixed with 10% formalin, embedded in paraffin, and sliced (thickness: 4 μm). The sliced tissues were then stained using hematoxylin and eosin (H&E) and observed using a digital microscope (Olympus BX41).

4.8. Statistical Analysis. Data were expressed as mean ± sd. Differences between groups were assessed by one-way ANOVA with Tukey multiple comparison tests. $p > 0.05$ means not significant (NS). $^*p < 0.05$ was considered significant, and $^{**}p < 0.01$, $^{***}p < 0.001$ were considered highly significant.

■ ASSOCIATED CONTENT

Supporting Information

The Supporting Information is available free of charge on the ACS Publications website at DOI: 10.1021/acs.chemmater.7b02953.

Materials; characterization; synthesis of copolymers Anis-PEG-P(HPMA-LA)-PAA, PEG-P(HPMA-LA)-PAA, and Cy5-NH_2-labeled PEG-P(HPMA-LA)-PAA; preparation of FITC or Cy5-labeled cytochrome C; loading and reduction-triggered release of FITC-CC from polymersomes; blood circulation of Anis-BCPs-Cy5; and preliminary *in vivo* antitumor experiments of GrB-Anis-BCPs (PDF)

■ AUTHOR INFORMATION

Corresponding Authors

*E-mail: fhmeng@suda.edu.cn.
*E-mail: zyzhong@suda.edu.cn.

ORCID

Fenghua Meng: 0000-0002-8608-7738
Zhiyuan Zhong: 0000-0003-4175-4741

Notes

The authors declare no competing financial interest.

■ ACKNOWLEDGMENTS

This work is financially supported by the National Natural Science Foundation of China (NSFC 51473111, 51561135010, 51633005, 51773146), the Major Program of the Natural Science Foundation of Jiangsu Province (14KJA150008), and Ph.D. Programs Foundation of Ministry of Education of China (20133201110005).

■ REFERENCES

(1) Lu, Y.; Sun, W.; Gu, Z. Stimuli-responsive nanomaterials for therapeutic protein delivery. *J. Controlled Release* **2014**, *194*, 1−19.

(2) Baselga, J.; Bradbury, I.; Eidtmann, H.; Di Cosimo, S.; de Azambuja, E.; Aura, C.; Gómez, H.; Dinh, P.; Fauria, K.; Van Dooren, V.; et al. Lapatinib with trastuzumab for HER2-positive early breast cancer (NeoALTTO): a randomised, open-label, multicentre, phase 3 trial. *Lancet* **2012**, *379*, 633−640.

(3) Stuckey, D. W.; Shah, K. TRAIL on trial: preclinical advances in cancer therapy. *Trends Mol. Med.* **2013**, *19*, 685−694.

(4) Czabotar, P. E.; Lessene, G.; Strasser, A.; Adams, J. M. Control of apoptosis by the BCL-2 protein family: implications for physiology and therapy. *Nat. Rev. Mol. Cell Biol.* **2014**, *15*, 49−63.

(5) Mo, R.; Jiang, T.; Di, J.; Tai, W.; Gu, Z. Emerging micro- and nanotechnology based synthetic approaches for insulin delivery. *Chem. Soc. Rev.* **2014**, *43*, 3595−3629.

(6) Pisal, D. S.; Kosloski, M. P.; Baluiyer, S. V. Delivery of therapeutic proteins. *J. Pharm. Sci.* **2010**, *99*, 2557−2575.

(7) Gu, Z.; Biswas, A.; Zhao, M.; Tang, Y. Tailoring nanocarriers for intracellular protein delivery. *Chem. Soc. Rev.* **2011**, *40*, 3638−3655.

(8) Tang, R.; Kim, C. S.; Solfiell, D. J.; Rana, S.; Mout, R.; Velázquezdelgado, E. M.; Chompoosor, A.; Jeong, Y.; Yan, B.; Zhu, Z. J.; et al. Direct delivery of functional proteins and enzymes to the cytosol using nanoparticle-stabilized nanocapsules. *ACS Nano* **2013**, *7*, 6667−6673.

(9) Liang, K.; Such, G. K.; Zhu, Z.; Yan, Y.; Lomas, H.; Caruso, F. Charge-Shifting Click Capsules with Dual-Responsive Cargo Release Mechanisms. *Adv. Mater.* **2011**, *23*, H273−H277.

(10) Deng, Z.; Qian, Y.; Yu, Y.; Liu, G.; Hu, J.; Zhang, G.; Liu, S. Y. Engineering Intracellular Delivery Nanocarriers and Nanoreactors from Oxidation-Responsive Polymersomes via Synchronized Bilayer Cross-Linking and Permeabilizing Inside Live Cells. *J. Am. Chem. Soc.* **2016**, *138*, 10452−10466.

(11) Fang, Y.; Jiang, Y.; Zou, Y.; Meng, F. H.; Zhang, J.; Deng, C.; Sun, H. L.; Zhong, Z. Y. Targeted glioma chemotherapy by cyclic RGD peptide-functionalized reversibly core-crosslinked multifunctional poly(ethylene glycol)-b-poly(ε-caprolactone) micelles. *Acta Biomater.* **2017**, *50*, 396−406.

(12) Zhao, M.; Hu, B.; Gu, Z.; Joo, K.-I.; Wang, P.; Tang, Y. Degradable polymeric nanocapsule for efficient intracellular delivery of a high molecular weight tumor-selective protein complex. *Nano Today* **2013**, *8*, 11−20.

(13) Kim, S. K.; Foote, M. B.; Huang, L. The targeted intracellular delivery of cytochrome C protein to tumors using lipid-apolipoprotein nanoparticles. *Biomaterials* **2012**, *33*, 3959−3966.

(14) Shin, S.-H.; Lee, J.; Lim, K. S.; Rhim, T.; Lee, S. K.; Kim, Y.-H.; Lee, K. Y. Sequential delivery of TAT-HSP27 and VEGF using microsphere/hydrogel hybrid systems for therapeutic angiogenesis. *J. Controlled Release* **2013**, *166*, 38−45.

(15) Rahimian, S.; Kleinovink, J. W.; Fransen, M. F.; Mezzanotte, L.; Gold, H.; Wisse, P.; Overkleeft, H.; Amidi, M.; Jiskoot, W.; Lowik, C. W.; Ossendorp, F.; Hennink, W. E. Near-infrared labeled, ovalbumin loaded polymeric nanoparticles based on a hydrophilic polyester as model vaccine: In vivo tracking and evaluation of antigen-specific CD8+ T cell immune response. *Biomaterials* **2015**, *37*, 469−477.

(16) Chung, J. E.; Tan, S.; Gao, S. J.; Kurisawa, M.; Ying, J. Y.; et al. Self-assembled micellar nanocomplexes comprising green tea catechin derivatives and protein drugs for cancer therapy. *Nat. Nanotechnol.* **2014**, *9*, 907−912.

(17) Wang, M.; Alberti, K.; Sun, S.; Arellano, C. L.; Xu, Q. Combinatorially designed lipid-like nanoparticles for intracellular delivery of cytotoxic protein for cancer therapy. *Angew. Chem., Int. Ed.* **2014**, *53*, 2893−2898.

(18) Li, D.; Kordalivand, N.; Fransen, M. F.; Ossendorp, F.; Raemdonck, K.; Vermonden, T.; Hennink, W. E.; Van Nostrum, C. F. Reduction-sensitive dextran nanogels aimed for intracellular delivery of antigens. *Adv. Funct. Mater.* **2015**, *25*, 2993−3003.

(19) Wu, X.; He, C.; Wu, Y.; Chen, X.; Cheng, J. Nanogel-incorporated physical and chemical hybrid gels for highly effective chemo-protein combination therapy. *Adv. Funct. Mater.* **2015**, *25*, 6744−6755.

(20) Tian, H.; Du, J.; Montgomery, S. R.; Wang, J. C.; Lu, Y.; et al. Growth-factor nanocapsules that enable tunable controlled release for bone regeneration. *ACS Nano* **2016**, *10*, 7362−7369.

(21) Won, Y.-W.; Yoon, S.-M.; Sonn, C. H.; Lee, K.-M.; Kim, Y.-H. Nano self-assembly of recombinant human gelatin conjugated with α-tocopheryl succinate for Hsp90 inhibitor, 17-AAG, delivery. *ACS Nano* **2011**, *5*, 3839−3848.

DOI: 10.1021/acs.chemmater.7b02953
Chem. Mater. 2017, 29, 8757−8765

(22) Yang, Y.; Wan, J.; Niu, Y.; Gu, Z.; Zhang, J.; Yu, M.; Yu, C. Structure-dependent and glutathione-responsive biodegradable dendritic mesoporous organosilica nanoparticles for safe protein delivery. *Chem. Mater.* **2016**, *28*, 9008−9016.
(23) Liang, K.; Richardson, J. J.; Ejima, H.; Such, G. K.; Cui, J.; Caruso, F. Peptide-tunable drug cytotoxicity via one-step assembled polymer nanoparticles. *Adv. Mater.* **2014**, *26*, 2398−2402.
(24) Chen, J.; Zou, Y.; Deng, C.; Meng, F. H.; Zhang, J.; Zhong, Z. Y. Multifunctional click hyaluronic acid nanogels for targeted protein delivery and effective cancer treatment *in vivo*. *Chem. Mater.* **2016**, *28*, 8792−8799.
(25) Kamat, N. P.; Robbins, G. P.; Rawson, J.; Therien, M. J.; Dmochowski, I. J.; Hammer, D. A. A generalized system for photoresponsive membrane rupture in polymersomes. *Adv. Funct. Mater.* **2010**, *20*, 2588−2596.
(26) Tanner, P.; Baumann, P.; Enea, R.; Onaca, O.; Palivan, C.; Meier, W. Polymeric vesicles: from drug carriers to nanoreactors and artificial organelles. *Acc. Chem. Res.* **2011**, *44*, 1039−1049.
(27) Oliveira, H.; Pérez-Andrés, E.; Thevenot, J.; Sandre, O.; Berra, E.; Lecommandoux, S. Magnetic field triggered drug release from polymersomes for cancer therapeutics. *J. Controlled Release* **2013**, *169*, 165−170.
(28) Liu, G.; Wang, X.; Hu, J.; Zhang, G.; Liu, S. Self-immolative polymersomes for high-efficiency triggered release and programmed enzymatic reactions. *J. Am. Chem. Soc.* **2014**, *136*, 7492−7497.
(29) Discher, D. E.; Ortiz, V.; Srinivas, G.; Klein, M. L.; Kim, Y.; Christian, D.; Cai, S.; Photos, P.; Ahmed, F. Emerging applications of polymersomes in delivery: from molecular dynamics to shrinkage of tumors. *Prog. Polym. Sci.* **2007**, *32*, 838−857.
(30) Zou, T.; Dembele, F.; Beugnet, A.; Sengmanivong, L.; Trepout, S.; Marco, S.; de Marco, A.; Li, M.-H. Nanobody-functionalized PEG-b-PCL polymersomes and their targeting study. *J. Biotechnol.* **2015**, *214*, 147−155.
(31) Saraswathy, M.; Gong, S. Recent developments in the co-delivery of siRNA and small molecule anticancer drugs for cancer treatment. *Mater. Today* **2014**, *17*, 298−306.
(32) Yin, H.; Kanasty, R. L.; Eltoukhy, A. A.; Vegas, A. J.; Dorkin, J. R.; Anderson, D. G. Non-viral vectors for gene-based therapy. *Nat. Rev. Genet.* **2014**, *15*, 541−555.
(33) Scott, E. A.; Stano, A.; Gillard, M.; Maio-Liu, A. C.; Swartz, M. A.; Hubbell, J. A. Dendritic cell activation and T cell priming with adjuvant- and antigen-loaded oxidation-sensitive polymersomes. *Biomaterials* **2012**, *33*, 6211−6219.
(34) Christian, D. A.; Cai, S.; Bowen, D. M.; Kim, Y.; Pajerowski, J. D.; Discher, D. E. Polymersome carriers: from self-assembly to siRNA and protein therapeutics. *Eur. J. Pharm. Biopharm.* **2009**, *71*, 463−474.
(35) Van Dongen, S. F.; Verdurmen, W. P.; Peters, R. J.; Nolte, R. J.; Brock, R.; van Hest, J. C. Cellular integration of an enzyme-loaded polymersome nanoreactor. *Angew. Chem., Int. Ed.* **2010**, *49*, 7213−7216.
(36) Li, X.; Yang, W. J.; Zou, Y.; Meng, F. H.; Deng, C.; Zhong, Z. Y. Efficacious delivery of protein drugs to prostate cancer cells by PSMA-targeted pH-responsive chimaeric polymersomes. *J. Controlled Release* **2015**, *220*, 704−714.
(37) Wang, X. Y.; Sun, H. L.; Meng, F. H.; Cheng, R.; Deng, C.; Zhong, Z. Y. Galactose-decorated reduction-sensitive degradable chimaeric polymersomes as a multifunctional nanocarrier to efficiently chaperone apoptotic proteins into hepatoma cells. *Biomacromolecules* **2013**, *14*, 2873−2882.
(38) Duncan, R.; Vicent, M. J. Do HPMA copolymer conjugates have a future as clinically useful nanomedicines? A critical overview of current status and future opportunities. *Adv. Drug Delivery Rev.* **2010**, *62*, 272−282.
(39) Park, S.; Karunakaran, U.; Jeoung, N. H.; Jeon, J. H.; Lee, I. K. Physiological effect and therapeutic application of alpha lipoic acid. *Curr. Med. Chem.* **2014**, *21*, 3636−3645.
(40) Maczurek, A.; Hager, K.; Kenklies, M.; Sharman, M.; Martins, R.; Engel, J.; Carlson, D. A.; Münch, G. Lipoic acid as an anti-inflammatory and neuroprotective treatment for Alzheimer's disease. *Adv. Drug Delivery Rev.* **2008**, *60*, 1463−1470.
(41) Zhong, Y. N.; Zhang, J.; Cheng, R.; Deng, C.; Meng, F. H.; Xie, F.; Zhong, Z. Y. Reversibly crosslinked hyaluronic acid nanoparticles for active targeting and intelligent delivery of doxorubicin to drug resistant CD44+ human breast tumor xenografts. *J. Controlled Release* **2015**, *205*, 144−154.
(42) Li, Y. L.; Zhu, L.; Liu, Z. Z.; Cheng, R.; Meng, F. H.; Cui, J. H.; Ji, S. J.; Zhong, Z. Y. Reversibly stabilized multifunctional dextran nanoparticles efficiently deliver doxorubicin into the nuclei of cancer cells. *Angew. Chem., Int. Ed.* **2009**, *48*, 9914−9918.
(43) Guo, J.; Ogier, J. R.; Desgranges, S.; Darcy, R.; O'Driscoll, C. Anisamide-targeted cyclodextrin nanoparticles for siRNA delivery to prostate tumours in mice. *Biomaterials* **2012**, *33*, 7775−7784.
(44) Della Rocca, R. J.; Huxford, R. C.; Comstock-Duggan, E.; Lin, W. Polysilsesquioxane nanoparticles for targeted platin-based cancer chemotherapy by triggered release. *Angew. Chem., Int. Ed.* **2011**, *50*, 10330−10334.
(45) Yang, W. J.; Zou, Y.; Meng, F. H.; Zhang, J.; Cheng, R.; Deng, C.; Zhong, Z. Y. Efficient and targeted suppression of human lung tumor xenografts in mice with methotrexate sodium encapsulated in all-function-in-one chimeric polymersomes. *Adv. Mater.* **2016**, *28*, 8234−8239.
(46) Cui, J.; Han, Y.; Jiang, W. Asymmetric vesicle constructed by AB/CB diblock copolymer mixture and its behavior: a Monte Carlo study. *Langmuir* **2014**, *30*, 9219−9227.
(47) Kim, S. K.; Huang, L. Nanoparticle delivery of a peptide targeting EGFR signaling. *J. Controlled Release* **2012**, *157*, 279−286.
(48) Lu, L.; Zou, Y.; Yang, W. J.; Meng, F. H.; Deng, C.; Cheng, R.; Zhong, Z. Y. Anisamide-decorated pH-sensitive degradable chimaeric polymersomes mediate potent and targeted protein delivery to lung cancer cells. *Biomacromolecules* **2015**, *16*, 1726−1735.
(49) Liu, Y.; Zhang, W.; Niu, T.; Cheung, L. H.; Munshi, A.; Meyn, R. E., Jr.; Rosenblum, M. G. Targeted apoptosis activation with GrB/scFvMEL modulates melanoma growth, metastatic spread, chemosensitivity, and radiosensitivity. *Neoplasia* **2006**, *8*, 125−135.
(50) Zhao, M.; Liu, Y.; Hsieh, R. S.; Wang, N.; Tai, W.; Joo, K. I.; Wang, P.; Gu, Z.; Tang, Y. Clickable protein nanocapsules for targeted delivery of recombinant p53 protein. *J. Am. Chem. Soc.* **2014**, *136*, 15319−15325.
(51) Cafforio, P.; Dammacco, F.; Gernone, A.; Silvestris, F. Statins activate the mitochondrial pathway of apoptosis in human lymphoblasts and myeloma cells. *Carcinogenesis* **2005**, *26*, 883−891.
(52) Ow, Y.-L. P.; Green, D. R.; Hao, Z.; Mak, T. W. Cytochrome c: functions beyond respiration. *Nat. Rev. Mol. Cell Biol.* **2008**, *9*, 532−542.
(53) Zhao, J.; Zhang, L. H.; Jia, L. T.; Zhang, L.; Xu, Y. M.; Wang, Z.; Yu, C. J.; Peng, W. D.; Wen, W. H.; Wang, C. J.; et al. Secreted antibody/granzyme B fusion protein stimulates selective killing of HER2-overexpressing tumor cells. *J. Biol. Chem.* **2004**, *279*, 21343−21348.
(54) Mohamedali, K. A.; Cao, Y.; Cheung, L. H.; Hittelman, W. N.; Rosenblum, M. G. The functionalized human serine protease granzyme B/$VEGF_{121}$ targets tumor vasculature and ablates tumor growth. *Mol. Cancer Ther.* **2013**, *12*, 2055−2066.

DOI: 10.1021/acs.chemmater.7b02953
Chem. Mater. 2017, 29, 8757−8765